Mon. Not. R. Astron. Soc. **260,** 191–201 (1993)

Simple galaxy models with massive haloes

N. W. Evans[1,2]

[1]*Department of Applied Mathematics and Theoretical Physics, Silver Street, Cambridge CB3 9EW*
[2]*Institute of Astronomy, Madingley Road, Cambridge CB3 0HA*

Accepted 1992 June 22. Received 1992 June 22; in original form 1992 May 12

ABSTRACT

The axisymmetric logarithmic potential introduced by Binney as a simple model of a galactic halo has an elementary distribution function depending on the two classical integrals of motion, binding energy E and angular momentum parallel to the symmetry axis L_z. The spherical limit is an isothermal distribution of two stellar populations whose masses and central densities are in the ratio 1:2.

It is more realistic to build composite models, in which a luminous component is embedded within a massive dark halo. The gravitational potentials of the dark matter and the stars are together the axisymmetric logarithmic potential. Pleasingly simple galaxies are generated by taking the distribution function of the luminous component to be an isothermal. The luminosity density is then stratified on similar concentric spheroids and can fall off asymptotically like r^{-3} or $r^{-3.5}$, as is appropriate for modelling elliptical galaxies and bulges. The kinematics are isotropic and the observables – the isophotes and line-of-sight second moment – are all simple. The surface brightness is a reasonable fit to the de Vaucouleurs profile. The non-rotating models have line profiles, or distributions of line-of-sight velocities, that are everywhere exactly Gaussian. The distortions to the line profiles caused by rotation are investigated by building distribution functions for three different rotation laws. The maximum deviation from Gaussian occurs for the maximum streaming model.

At a slight cost in mathematical simplicity, it is possible to construct luminous components with anisotropic kinematics in the dark halo by modifying the isothermal distribution function. The observables and projected quantities are still elementary functions. The line profile is given for models with and without rotation.

Key words: celestial mechanics, stellar dynamics – galaxies: elliptical and lenticular, cD – galaxies: kinematics and dynamics – galaxies: structure.

1 INTRODUCTION

In physics, analytical formulae are only really useful when simple! For example, Binney's (1981) axisymmetric logarithmic potential has found widespread applications in stellar dynamics as an elegant yet realistic model of a galactic halo (see, for example, Binney & Tremaine 1987). The density falls like r^{-2} at large radii and the equipotentials are exactly spheroidal. The model combines simplicity with a high degree of astrophysical accuracy.

Even today, axisymmetric potential–density pairs with elementary distribution functions are extraordinarily scarce. There are only two known models with breathtakingly simple distribution functions. The first is the axisymmetric Plummer family devised by Lynden-Bell (1962) and subsequently extended by Hunter (1975) and Lake (1981). The second is Toomre's (1982) scale-free family, for which the distribution functions are elementary and the density (in general) vanishes on the symmetry axis.

The purpose of this paper is to point out that Binney's logarithmic potential also has a simple distribution function depending on the two classical integrals of binding energy E and angular momentum parallel to the symmetry axis L_z. Even better, composite models of luminous material embedded within the massive halo with any asymptotic density decay can be built very easily.

2 THE LOGARITHMIC POTENTIAL

Using cylindrical polar coordinates (R, ϕ, z), the axisymmetric logarithmic potential is

$$\psi = -\frac{1}{2} v_0^2 \log\left(R_c^2 + R^2 + \frac{z^2}{q^2}\right) \tag{2.1}$$

(Binney 1981; Binney & Tremaine 1987), where R_c is the core radius and q is the axial ratio of the spheroidal equipotentials. The density generated through Poisson's equation is

$$\rho(R, z) = \frac{v_0^2}{4\pi G q^2} \frac{(2q^2+1)R_c^2 + R^2 + (2-q^{-2})z^2}{(R_c^2 + R^2 + z^2 q^{-2})^2}, \tag{2.2}$$

which can be written as

$$\rho(R, \psi) = \frac{v_0^2}{4\pi G q^2} [2(1-q^2)R^2 \exp(4\psi/v_0^2) + 2R_c^2 \exp(4\psi/v_0^2) + (2q^2-1)\exp(2\psi/v_0^2)]. \tag{2.3}$$

The stars orbiting in the model possess two classical integrals of motion, namely the binding energy E and the component of angular momentum L_z. Lynden-Bell (1962) showed that the unique even part of the distribution function $F(E, L_z^2)$ can be recovered from $\rho(R, \psi)$ by a double Laplace inversion. Application of his method gives

$$F(E, L_z^2) = A L_z^2 \exp(4E/v_0^2) + B \exp(4E/v_0^2) + C \exp(2E/v_0^2), \tag{2.4}$$

where A, B and C are constants

$$A = \left(\frac{2}{\pi}\right)^{5/2} \frac{(1-q^2)}{G q^2 v_0^3}, \qquad B = \left(\frac{2}{\pi^5}\right)^{1/2} \frac{R_c^2}{G q^2 v_0}, \qquad C = \frac{2q^2-1}{4\pi^{5/2} G q^2 v_0}. \tag{2.5}$$

This (2.4) is an *unbelievably simple* result. The very few axisymmetric models with distribution functions are collected in Dejonghe (1986) and Hunter & Qian (1993). A glance through these papers shows that generally axisymmetric galaxies can only be built with distribution functions that are at least higher transcendental functions!

The prolate mass models with $q > 1.08$ are unphysical, as the distribution function is not positive definite. For the oblate models, the distribution is everywhere positive if and only if $q \geq 1/\sqrt{2} = 0.707$, i.e. exactly the value inferred from the density profile on the z-axis in Binney & Tremaine (1987). Note that, in the limit of vanishing core radius R_c, the logarithmic potential becomes scale-free and Toomre's (1982) result is recovered. Only in the parameter range $0.707 \leqslant q \leqslant 1.08$ does the axisymmetric logarithmic potential generate physically acceptable models.

The second moments are readily found by direct integration over velocity space as

$$\langle v_R^2 \rangle = \langle v_z^2 \rangle = \frac{v_0^2}{2} \frac{2q^2 R_c^2 + q^2 R^2 + (2-q^{-2})z^2}{(2q^2+1)R_c^2 + R^2 + (2-q^{-2})z^2}, \tag{2.6}$$

$$\langle v_\phi^2 \rangle = \frac{v_0^2}{2} \frac{2q^2 R_c^2 + (2-q^2)R^2 + (2-q^{-2})z^2}{(2q^2+1)R_c^2 + R^2 + (2-q^{-2})z^2}. \tag{2.7}$$

A direct consequence of the dependence of the distribution function only on E and L_z is that all the mixed second moments vanish and so the velocity ellipsoid is oriented on cylindrical polar coordinate surfaces. Fig. 1(a) plots the velocity ellipsoids in a meridional plane for the $q = 0.80$ model. The dashed circles are sections with the $(\sqrt{\langle v_R^2 \rangle}, \sqrt{\langle v_z^2 \rangle})$ plane, the full ellipses sections with the $(\sqrt{\langle v_\phi^2 \rangle}, \sqrt{\langle v_z^2 \rangle})$ plane. Logarithmic contours of constant density are drawn in broken lines.

When the model is viewed at inclination angle i ($i = 90°$ is edge-on), the projected surface density Σ on the plane of the sky (x', y') is

$$\Sigma(x', y') = \frac{v_0^2 q}{4G} \frac{x'^2 + y'^2 + R_c^2(1 + \cos^2 i + q^2 \sin^2 i)}{[(x'^2 + R_c^2)(\cos^2 i + q^2 \sin^2 i) + y'^2]^{3/2}}. \tag{2.8}$$

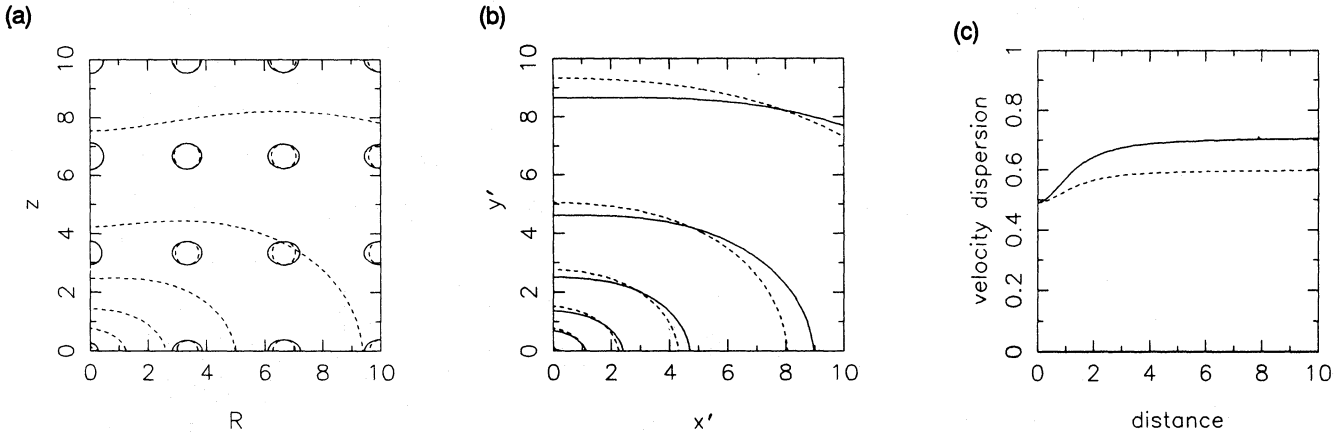

Figure 1. (a) The velocity ellipsoids for the $q=0.80$ axisymmetric logarithmic potential. Dashed circles are sections with the $(\sqrt{\langle v_R^2\rangle}, \sqrt{\langle v_z^2\rangle})$ plane, full ellipses are sections with the $(\sqrt{\langle v_\phi^2\rangle}, \sqrt{\langle v_z^2\rangle})$ plane. Logarithmic isocontours of constant density are shown in broken lines. Units are chosen so that $G=R_c=v_0=1$. (b) The logarithmic contours of surface density for this model viewed edge-on (full line) and at an inclination of 60° (broken line). (c) The line-of-sight dispersion $\sqrt{\langle v_{los}^2\rangle}$ of this model plotted against distance along the isophotal major and minor axes (full and broken lines respectively).

Fig. 1(b) shows logarithmic contours of constant surface density for the $q=0.80$ model at inclinations $i=90°$ (full line) and $i=60°$ (broken line). The central and asymptotic axis ratios of the contours of surface density are

$$\left(\frac{a_1^2}{a_2^2}\right)_0=\frac{3+\cos^2 i+q^2\sin^2 i}{(\cos^2 i+q^2\sin^2 i)(1+3\cos^2 i+3q^2\sin^2 i)}, \qquad \left(\frac{a_1}{a_2}\right)_\infty=\frac{1}{(\cos^2 i+q^2\sin^2 i)^{3/2}}. \tag{2.9}$$

The ellipticity increases somewhat outwards. The line-of-sight second moment $\langle v_{los}^2\rangle$ is

$$\langle v_{los}^2\rangle=\frac{v_0^2}{4}\frac{ax'^2+by'^2+cR_c^2}{x'^2+y'^2+R_c^2(1+\cos^2 i+q^2\sin^2 i)}, \tag{2.10}$$

where

$$a=2+(1-q^{-2})\cos^2 i+2(q^2+q^{-2}-2)\sin^2 i\cos^2 i, \qquad b=3-q^{-2}, \qquad c=3q^2+(4-3q^2-q^{-2})\cos^2 i. \tag{2.11}$$

Fig. 1(c) shows the line-of-sight velocity dispersion $\sqrt{\langle v_{los}^2\rangle}$ along the isophotal major and minor axes (the full and broken lines respectively) for the $q=0.80$ model viewed edge-on. The dip near the centre is caused by the mass concentration there.

Finally, in the spherical limit $q=1$, the potential–density pair becomes

$$\psi=-\frac{1}{2}v_0^2\log(r^2+R_c^2), \qquad \rho=\frac{v_0^2}{4\pi G}\frac{r^2+3R_c^2}{(r^2+R_c^2)^2}, \tag{2.12}$$

while the distribution function is

$$F=B\exp(4E/\psi_0^2)+C\exp(2E/v_0^2). \tag{2.13}$$

This is an isothermal distribution of two stellar populations whose masses and central densities are in the ratio 1:2. The spherical end-point of Binney's logarithmic model is thus a *non-singular isothermal sphere.*

3 COMPOSITE MODELS

The self-consistent problem of stellar dynamics is to find the distribution function F compatible with a prescribed potential–density pair. However, the distributions of stars in our own Galaxy vary from class to class – it is the sum of the distribution functions of the O stars, and the B stars, and so on, which generates the global potential–density pair. It is not each component, but rather the sum of all the components, that is a self-consistent solution of the Poisson and Vlasov equations. Such systems we call *composite models.*

The simplest composite model of a galaxy is built from just two components, stars and dark matter. In the core, most of the mass density is in the stars, while dark matter dominates in the far field. Let us suppose the density of luminous material

embedded within a massive dark halo is

$$\rho_{\rm luminous}=\frac{\rho_0 R_{\rm c}^p}{(R_{\rm c}^2+R^2+z^2q^{-2})^{p/2}}, \tag{3.1}$$

where ρ_0 is the central density and $p\geq 2$ prescribes the asymptotic density decay. Together, the luminous material and the dark matter generate the potential (2.1) and the density (2.2). The mass-to-light ratio Y is

$$\Upsilon(R,z)=\frac{\rho_{\rm luminous}+\rho_{\rm dark}}{\rho_{\rm luminous}}=\frac{v_0^2}{4\pi G\rho_0 q^2 R_{\rm c}^p}[(2q^2+1)R_{\rm c}^2+R^2+(2-q^{-2})z^2](R_{\rm c}^2+R^2+z^2q^{-2})^{(p-4)/2}, \tag{3.2}$$

which grows asymptotically like r^{p-2}. Both the components have elementary distribution functions, namely

$$F_{\rm dark}=AL_z^2\exp(4E/v_0^2)+B\exp(4E/v_0^2)+C\exp(2E/v_0^2)-D\exp(pE/v_0^2), \tag{3.3}$$

$$F_{\rm luminous}=D\exp(pE/v_0^2), \tag{3.4}$$

where D is a constant

$$D=\rho_0 R_{\rm c}^p\left(\frac{p}{2\pi v_0^2}\right)^{3/2}. \tag{3.5}$$

Notice that (3.4) is exactly Boltzmann's formula in classical statistical physics. A gas with molecular mass m and temperature T in the axisymmetric logarithmic potential (2.1) settles to the very same spheroidal density distribution (3.1), but with index $p=mv_0^2/kT$ (k is Boltzmann's constant). In the composite model, the level sets of the luminosity density coincide with the global equipotentials and the shining material forms an exactly isothermal self-gravitating spheroid. The restriction that the phase space density of each component is positive definite is discussed in Appendix A.

As the distribution function of the luminous matter depends only on the binding energy, the velocity dispersion tensor is isotropic. Direct integration over velocity space yields the remarkable conclusion that all the second moments are everywhere equal to the same value, i.e.

$$\langle v_R^2\rangle=\langle v_z^2\rangle=\langle v_\phi^2\rangle=\frac{v_0^2}{p}. \tag{3.6}$$

For $p>3$, the total mass of luminous matter is finite and given by

$$M=\frac{2^{p-3}B[(p-3)/2,(p-3)/2]\pi\rho_0 q R_{\rm c}^3}{p-2}, \tag{3.7}$$

where B is the beta function. The total kinetic energy of the luminous matter is

$$T=\frac{1}{2}\sum_{i=1}^{3}\int\rho\langle v_i^2\rangle\,{\rm d}V=\frac{3Mv_0^2}{2p}. \tag{3.8}$$

The trace of the virial tensor (which is *not* equal to the total potential energy for a composite model) is

$$\Omega=\sum_{i=1}^{3}\int\rho x_i\frac{\partial\psi}{\partial x_i}\,{\rm d}V=-\frac{3Mv_0^2}{p}, \tag{3.9}$$

so that, in accord with the virial theorem, $2T+\Omega=0$.

The surface brightness $I(x',y')$ is found by integrating the luminosity density along the line of sight. The isophotes are similar concentric ellipses with axis ratios $a_2/a_1=(\cos^2 i+q^2\sin i)^{1/2}\doteq q'$. This is an immediate consequence of the stratification of the density on similar concentric spheroids with axial ratio q (Contopoulos, 1954). We find

$$I(x',y')=\frac{2^{p-2}B[(p-1)/2,(p-1)/2]q\rho_0 R_{\rm c}^p}{q'[x'^2+R_{\rm c}^2+q'^{-2}y'^2]^{(p-1)/2}}, \tag{3.10}$$

where, as before, (x',y') are coordinates on the plane of the sky. Notice that the instance $p=3$ is an axisymmetric extension of King's modification (Rood et al. 1972) of the Hubble (1930) profile. Fig. 2(a) plots the isophotes for the case when $p=3.5$ and

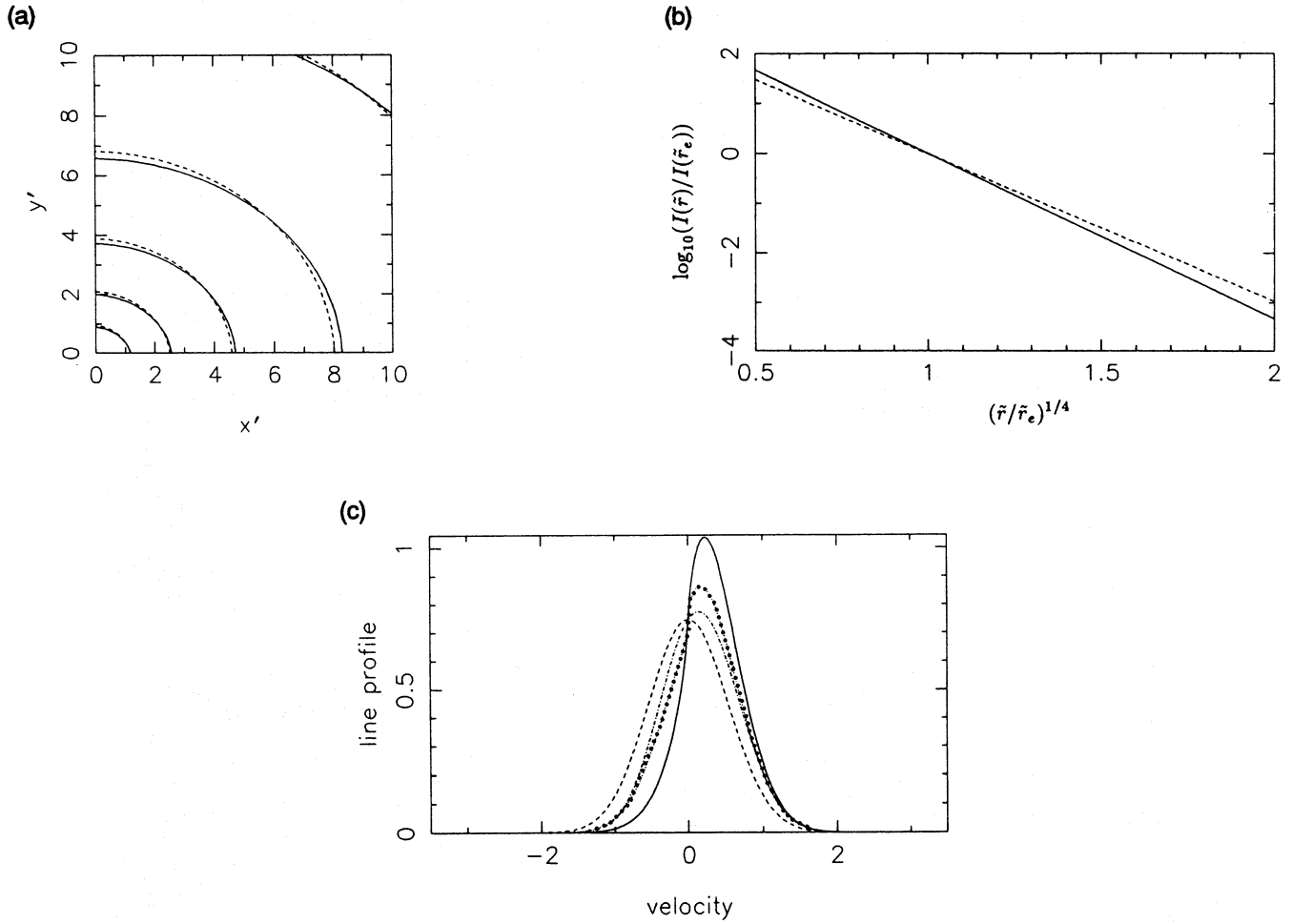

Figure 2. (a) Logarithmic isocontours of surface brightness for an isothermal composite model with $p=3.5$ and $q=0.80$ viewed edge-on (full lines) and at an inclination of 60° (broken lines). This is an E2 oblate spheroid, with density falling off like $r^{-3.5}$, embedded in a dark halo. (b) A plot of the logarithm of the surface brightness against $(\tilde{r}/\tilde{r}_e)^{1/4}$ for the de Vaucouleurs profile (full line) and the isothermal composite model with $p=3.5$ and $q=0.80$ (broken line). The surface brightness is normalized to its value at the effective radius. (c) The distribution of line-of-sight velocities (line profiles) for the $p=3.5$ and $q=0.80$ isothermal composite models described in Section 3. The full line corresponds to the maximum streaming model, the dashed line to a model without rotation. The dot–dashed line is the line profile for the rotation law (3.19), and the dotted line for the rotation law (3.22). The models are all observed edge-on at exactly one core radius R_c from the centre. The unit of velocity is v_0.

$q=0.80$ (an E2 oblate spheroid whose density falls off asymptotically like $r^{-3.5}$) viewed at inclinations $i=90°$ (full line) and $i=60°$ (broken line).

The cumulative surface brightness $S(\tilde{r})$ can be found as a function of elliptic radius $\tilde{r}^2=x'^2+q'^{-2}y'^2$. For $p>3$, it is

$$S(\tilde{r})=M\left[1-\left(\frac{R_c^2}{\tilde{r}^2+R_c^2}\right)^{(p-3)/2}\right]. \tag{3.11}$$

The effective radius $\tilde{r}_e$ defines the isophote that encloses half the light. Solving the equation $S(\tilde{r}_e)=M/2$, we find

$$\tilde{r}_e=R_c(2^{2/(p-3)}-1)^{1/2}. \tag{3.12}$$

For the $p=3.5$ and $q=0.80$ model viewed edge-on, $\tilde{r}_e=3.87R_c$. Fig. 2(b) compares the surface brightness of this model (broken line) with the empirical de Vaucouleurs profile (full line)

$$\log_{10}\left[\frac{I(\tilde{r})}{I(\tilde{r}_e)}\right]=-3.331\left[\left(\frac{\tilde{r}}{\tilde{r}_e}\right)^{1/4}-1\right], \tag{3.13}$$

which is known to provide an excellent fit to the luminosity distribution of elliptical galaxies and bulges (de Vaucouleurs 1948; Kormendy 1977). The graph shows the logarithm of the surface brightness normalized to its value at the effective radius plotted

against $(\tilde{r}/\tilde{r}_e)^{1/4}$. The agreement between the two laws is reasonably good. The surface brightness profiles agree to within ≈ 40 per cent for radii $0.06 \leq \tilde{r}/\tilde{r}_e \leq 13.0$, which enclose ≈ 85 per cent of the light. The largest discrepancies occur at the extremes of the range. Note that Jaffe (1987) and Binney (1988) have shown that de Vaucouleurs' law is closely related to models with density profiles $\rho \propto r^{-4}$ at large radii, and so the surface brightness of the $p=4$ model is an even better fit.

The projected line-of-sight second moment is incredibly simple,

$$\langle v_{\rm los}^2 \rangle = \frac{v_0^2}{p}, \tag{3.14}$$

and so is equal to the same constant value as any of the components of the velocity dispersion tensor (3.6), whatever the inclination angle or position on the plane of the sky!

Illingworth & Franx (1989) showed that there is valuable kinematic information in the line profiles $\ell(v_\parallel, x', y')$ – that is, the distribution of line-of-sight velocities $v_\parallel$ – derived from stellar absorption spectra. By integrating the distribution function along the line of sight and over the tangential velocity components, we find

$$\begin{aligned} \ell(v_\parallel, x', y') &= \frac{1}{I(x', y')} \int_{-\infty}^{\infty} {\rm d}s \int_{-\infty}^{\infty} {\rm d}v_{y'} \int_{-\infty}^{\infty} {\rm d}v_{x'} F_{\rm luminous}, \\ &= \left(\frac{p}{2\pi v_0^2} \right)^{1/2} \exp\left(-\frac{p v_\parallel^2}{2 v_0^2} \right), \end{aligned} \tag{3.15}$$

where we have normalized to unit surface brightness. The line profile is exactly Gaussian, which of course is a consequence of the Boltzmann form of the distribution function. Significant distortions from the Gaussian profile only occur for rotating models, which we now investigate.

For any stellar system, there is a maximum angular momentum state which may not be exceeded. It is constructed by Lynden-Bell's (1960) demon, who reverses the azimuthal velocities of all the, say, clockwise rotating stars. The rotating luminous component with maximum streaming has the distribution function

$$F_{\rm luminous} = \begin{cases} 2D \exp(pE/v_0^2), & \text{if } v_\phi > 0, \\ 0, & \text{if } v_\phi < 0. \end{cases} \tag{3.16}$$

The rotational velocity $\langle v_\phi \rangle$ is everywhere constant and equal to

$$\langle v_\phi \rangle = \left(\frac{2}{\pi p} \right)^{1/2} v_0, \tag{3.17}$$

and the semi-axes of the velocity ellipsoids are everywhere in the ratios $\sqrt{\langle v_R^2 \rangle} : \sqrt{\langle v_z^2 \rangle} : \sqrt{\langle v_\phi^2 \rangle - \langle v_\phi \rangle^2} = 1.66 : 1.66 : 1.00$. When the model is viewed edge-on, the line profile on the projected major axis is

$$\ell(v_\parallel, x', 0) = \left(\frac{p}{2\pi v_0^2} \right)^{1/2} \exp\left(-\frac{p v_\parallel^2}{2 v_0^2} \right) \left\{ 1 + \frac{(x'^2 + R_c^2)^{(p-1)/2}}{2^{p-3} B[(p-1)/2, (p-1)/2]} \int_0^{\infty} \frac{{\rm d}u \, {\rm erf}(\sqrt{p} v_\parallel x' / (\sqrt{2} v_0 u))}{(R_c^2 + x'^2 + u^2)^{p/2}} \right\}, \tag{3.18}$$

where ${\rm erf}(x)$ is the error function. The full and dashed curves in Fig. 2(c) are the line-of-sight velocities observed through a spectroscope positioned one core radius along the major and minor axis for the $p=3.5$ and $q=0.80$ model. The major axis line profile is much thinner and significantly lopsided. The mean line-of-sight velocity $\langle v_{\rm los} \rangle = 0.321\, v_0$ is consequently greater than the most common line-of-sight velocity of $0.237\, v_0$. The line-of-sight dispersion $\sigma_{\rm los}$, defined by $\sqrt{\langle v_{\rm los}^2 \rangle - \langle v_{\rm los} \rangle^2}$, is $0.427\, v_0$. By contrast, along the minor axis, the line profile is unchanged from the Gaussian (3.15), with $\langle v_{\rm los} \rangle = 0$ and dispersion $\sigma_{\rm los} = 0.534\, v_0$.

A systematic investigation of the effects of rotation on the line profile of the luminous component can be undertaken by deriving the part of the distribution function that is odd in the azimuthal velocity component v_ϕ. This determines the relative number of clockwise and anticlockwise rotating stars, which may vary without affecting the mass density. Lynden-Bell (1962) showed how to use double Laplace inversion to deduce the unique odd part of the distribution function $F^{\rm odd}(E, L_z)$ consistent with any rotation law $\langle v_\phi \rangle(R)$ of an axisymmetric galaxy. Suppose we prescribe

$$\langle v_\phi \rangle(R) = \frac{v_* R^2}{R_*^2 + R^2}, \tag{3.19}$$

which tends to zero in the core and to the constant value v_* when R is very much greater than the turn-over radius R_*. Then the odd part of the distribution function can be calculated as

$$F^{\rm odd}_{\rm luminous}=\frac{v_*p^2\rho_0R_{\rm c}^p}{4\pi v_0^4}\,{\rm sign}\,(L_z)\exp(pE/v_0^2)\left[1-\exp\left(-\frac{pL_z^2}{2R_*^2v_0^2}\right)\right], \tag{3.20}$$

and is added to the even part (3.4) to generate the full and *entirely elementary* distribution function. It is positive definite, providing v_* is less than the maximum streaming velocity (3.17). When viewed edge-on, the line profile on the major axis is modified from (3.18) to

$$\ell(v_\parallel,x',0)=\ell_{\rm max}(v_\parallel,x',0)-\left(\frac{p}{2\pi v_0^2}\right)^{1/2}\exp\left(-\frac{pv_\parallel^2}{2v_0^2}\right)\frac{R_{\rm c}(x'^2+R_{\rm c}^2)^{(p-1)/2}}{2^{p-3}B[(p-1)/2,(p-1)/2]}\times\int_0^\infty\frac{{\rm d}u\exp(-\eta^2)\,{\rm erf}(\eta R_{\rm c}/u)}{(u^2+R_{\rm c}^2)^{1/2}(u^2+x'^2+R_{\rm c}^2)^{p/2}}, \tag{3.21}$$

where $\eta=\sqrt{p}v_\parallel x'/(\sqrt{2(u^2+R_{\rm c}^2)}v_0)$. Here, we have denoted the rhs of (3.18) by $\ell_{\rm max}$, and set v_* to the maximum streaming velocity and R_* to the core radius $R_{\rm c}$. This lengthy expression is evaluated numerically and plotted in the dot–dashed line in Fig. 2(c). The mean line-of-sight velocity $\langle v_{\rm los}\rangle$ is $0.167\,v_0$, while the dispersion is $\sigma_{\rm los}=0.508\,v_0$. On the minor axis, the line profile is still just the Gaussian (3.15) with $\langle v_{\rm los}\rangle=0$ and $\sigma_{\rm los}=0.534\,v_0$.

An even more realistic rotation law is

$$\langle v_\phi\rangle(R)=\frac{v_*R}{R_*+R}, \tag{3.22}$$

which tends to solid-body rotation in the core and to the constant value v_* asymptotically. The odd part of the distribution function can again be found, but now involves special functions, namely

$$F^{\rm odd}_{\rm luminous}=\frac{v_*p^2\rho_0R_{\rm c}^p}{4\pi v_0^4}\,{\rm sign}\,(L_z)\exp(pE/v_0^2)\left[1-\exp\left(\frac{pL_z^2}{2R_*^2v_0^2}\right){\rm erfc}\left(\frac{\sqrt{p}|L_z|}{\sqrt{2}R_*v_0}\right)\right], \tag{3.23}$$

where ${\rm erfc}\,(x)=1-{\rm erf}\,(x)$ and v_* is not greater than the maximum streaming velocity (3.17). Two of the three quadratures to find the line profile can be performed analytically, the last one numerically. We omit the rather lengthy mathematical expression, but display the results in the dotted line in Fig. 2(c). Again, we have set v_* equal to the maximum streaming velocity and R_* equal to the core radius $R_{\rm c}$. The observer is viewing the model exactly edge-on and one core radius from the centre along the major axis. The mean line-of-sight velocity $\langle v_{\rm los}\rangle$ is now $0.186\,v_0$ and the dispersion is $\sigma_{\rm los}=0.501\,v_0$. On the minor axis, the line profile is the usual Gaussian (3.15).

It is physically plausible that the greatest deviation from Gaussian line profile occurs for the maximum streaming model. This is because at each point in the galaxy, we have taken as much out of the random motions and put it into streaming as we possibly can. This supposition is borne out by our numerical quadratures. On the minor axis, the incorporation of streaming makes no difference to the line profiles when viewed edge-on. This is because here, the rotation is transverse to the line of sight. Finally, we emphasize that although the expressions derived for our line profiles are indeed rather lengthy, in general the awkward triple integral has to be completely evaluated numerically with a consequent loss of accuracy. It is a measure of the striking simplicity of the models that the line profiles can be reduced to a single quadrature for so many rotation laws!

4 ANISOTROPIC COMPOSITE MODELS

Models in which the distribution function of the stars is isothermal are attractively simple. However, they suffer from two defects. First, the level surfaces of the density of the luminous material are rounder than those of the dark matter. This is the exact reverse of what we expect if the dark matter is dissipationless. Secondly, as $q\geq 1/\sqrt{2}=0.707$, the ellipticity of the luminous component cannot be greater than E3. We can evade these disadvantages by discarding the ansatz that the distribution function is an isothermal. Allowing it to depend explicitly on L_z as well as E enables the construction of flatter luminous components with anisotropic kinematics embedded within the dark halo.

Suppose the density of luminous material is taken as

$$\rho_{\rm luminous}=\frac{\rho_0R_{\rm c}^p(R_{\rm c}^2+s^{-2}R^2+q^{-2}z^2)}{(R_{\rm c}^2+R^2+q^{-2}z^2)^{(p+2)/2}}, \tag{4.1}$$

where $p \geq 2$ again prescribes the asymptotic density decay and $s < 1$ generates flattened oblate mass models. The results of Section 3 are recovered in the limit $s = 1$. At large radii, the axial ratio is

$$\left(\frac{a_1}{a_2}\right)_\infty = \frac{1}{qs^{2/p}}. \tag{4.2}$$

Choosing $p = s^{-2} = 3.5$ and $q = 0.80$ gives a luminous component with density falling off like $r^{-3.5}$ and with asymptotic ellipticity of 0.441 in a dark halo with axis ratio 0.80. Logarithmic isocontours of constant density are plotted in broken lines in Fig. 3(a). As s diminishes, the density contours become more oblate. If s becomes too small, however, the contours are toroidal, which is somewhat unphysical. With $p = 3.5$ and $q = 0.80$, the minimum realistic value of s corresponds to $s^{-2} = 6.5$ and an ellipticity at large radii of 0.531. Still flatter luminous models (such as E6) can be made by diminishing p and q.

The distribution generating the component (4.1) is again elementary, but no longer isothermal:

$$F_{\text{luminous}} = \tilde{A} L_z^2 \exp\left[(p+2)E/v_0^2\right] + \tilde{B} \exp\left(pE/v_0^2\right), \tag{4.3}$$

where $\tilde{A}$ and $\tilde{B}$ are the constants

$$\tilde{A} = \left(\frac{p+2}{v_0^2}\right)^{5/2} \frac{\rho_0 R_c^p (s^{-2}-1)}{(2\pi)^{3/2}}, \qquad \tilde{B} = \left(\frac{p}{2\pi v_0^2}\right)^{3/2} \rho_0 R_c^p. \tag{4.4}$$

The requirement that the distribution functions of the stars and the dark halo are positive definite is derived in Appendix A.

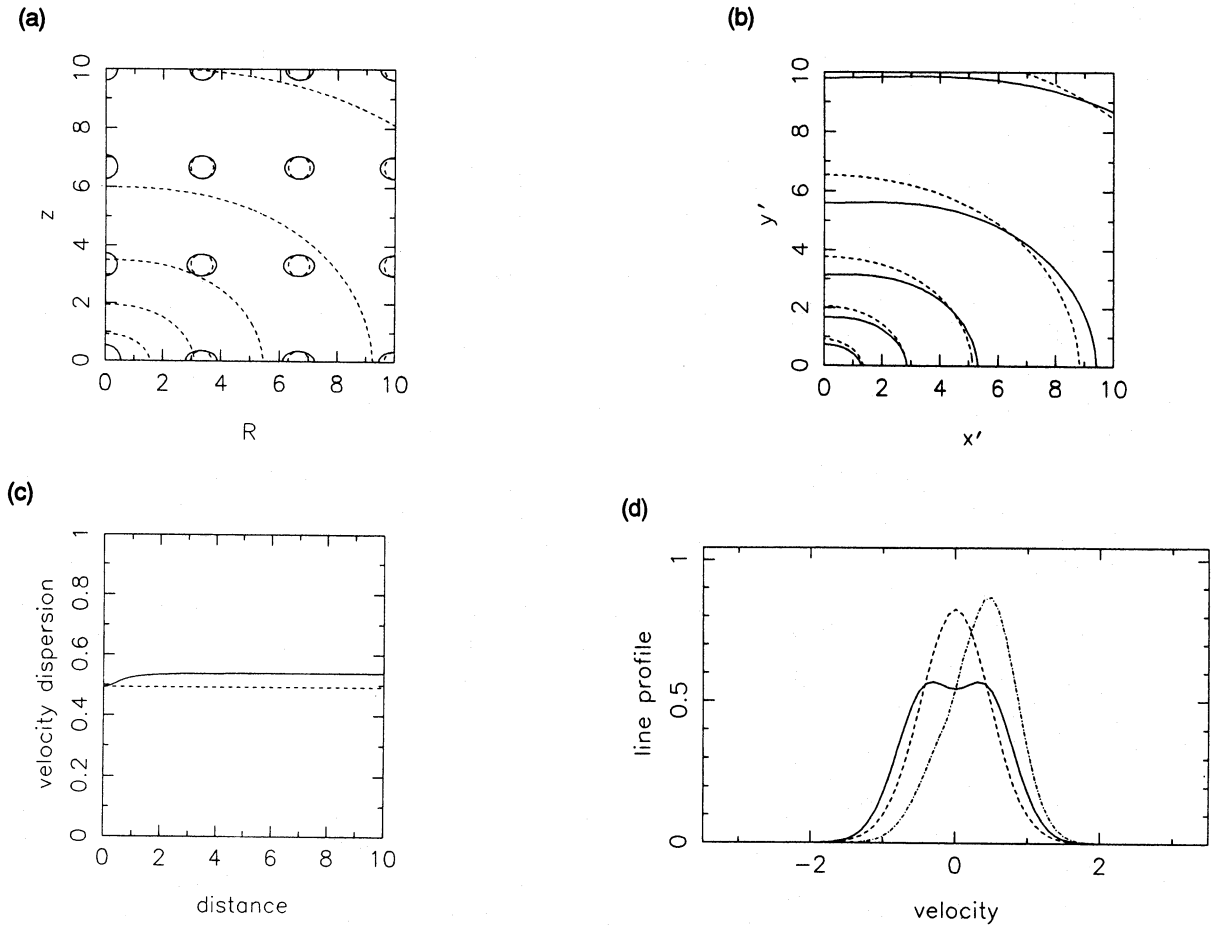

Figure 3. (a) The velocity ellipsoids for the $p = s^{-2} = 3.5$ and $q = 0.80$ anisotropic composite model. This is an E4.4 oblate spheroid, with density falling off like $r^{-3.5}$, embedded within a dark halo. Logarithmic isocontours of constant density are shown in broken lines. Units are chosen such that $\rho_0 = R_c = v_0 = 1$. (b) The logarithmic isocontours of surface brightness for this model viewed edge-on (full line) and at 60° inclination (broken line). (c) The line-of-sight dispersion $\sqrt{\langle v_{\text{los}}^2 \rangle}$ of this model plotted against distance along the isophotal major and minor axes (full and broken lines respectively). (d) The distribution of line-of-sight velocities (line profiles) for the $p = s^{-2} = 3.5$ and $q = 0.80$ anisotropic composite model. The full and dashed lines are the major and minor axis line profiles for a model without rotation. The dot-dashed line is the major axis line profile for the maximum streaming model. The models are all observed edge-on exactly one core radius from the centre. The unit of velocity is v_0.

Performing the integration over velocity space, the second moments are

$$\langle v_R^2\rangle=\langle v_z^2\rangle=\frac{v_0^2}{p}-\frac{2v_0^2(s^{-2}-1)R^2}{p(p+2)(R_c^2+s^{-2}R^2+q^{-2}z^{-2})}, \tag{4.5}$$

$$\langle v_\phi^2\rangle=\frac{v_0^2}{p}+\frac{2(p-1)v_0^2(s^{-2}-1)R^2}{p(p+2)(R_c^2+s^{-2}R^2+q^{-2}z^2)}. \tag{4.6}$$

The velocity ellipsoids are plotted in Fig. 3(a) for the $p=s^{-2}=3.5$ and $q=0.80$ model. The longest axis of the velocity ellipsoid points at right angles to the meridional planes. There is rough isotropy in the core, but as $R\to\infty$, the kinematics becomes more anisotropic. The mass and global virial quantities converge in the instance $p>3$ and are listed in Table 1. The observables – the isophotes and line-of-sight second moments – are lengthy expressions if derived at arbitrary inclination angles and so are given in the table for edge-on viewing only. Fig. 3(b) shows the isophotes for our usual $p=s^{-2}=3.5$ and $q=0.80$ model when viewed edge-on (full lines) and at an inclination angle of 60° (broken lines). Fig. 3(c) is a plot of the line-of-sight dispersion $\sqrt{\langle v_{los}^2\rangle}$ along the isophotal major and minor axes for edge-on observers.

The modification of the distribution function causes important changes to the line profiles of the model, which are now no longer simple Gaussians. On the major axis, we find the edge-on line profile is a sum of Gaussians multiplied by powers of $v_\parallel$, i.e.

$$\ell(v_\parallel,x',0)=\left(\frac{p}{2\pi v_0^2}\right)^{1/2}\frac{p(x'^2+R_c^2)}{ps^{-2}x'^2+(s^{-2}+p-1)R_c^2}\exp\left(-\frac{pv_\parallel^2}{2v_0^2}\right)$$
$$+\left(\frac{p+2}{2\pi v_0^6}\right)^{1/2}\frac{(s^{-2}-1)[x'^2(v_0^2+(p-1)(p+2)v_\parallel^2)+R_c^2v_0^2]}{ps^{-2}x'^2+(s^{-2}+p-1)R_c^2}\exp\left(-\frac{(p+2)v_\parallel^2}{2v_0^2}\right). \tag{4.7}$$

This is plotted in Fig. 3(d) (full line) assuming an observation point one core radius from the centre. Compared to the models of Section 3, the distribution function is now more strongly biased towards higher angular momentum orbits, which gives the double-humped shape to the line profile. The mean line-of-sight velocity $\langle v_{los}\rangle$ is zero, and the dispersion σ_{los} is $0.524v_0$. On the minor axis viewed edge-on, we find

$$\ell(v_\parallel,0,y')=\left(\frac{p}{2\pi v_0^2}\right)^{1/2}\frac{p}{s^{-2}+p-1}\exp\left(-\frac{pv_\parallel^2}{2v_0^2}\right)+\left(\frac{p+2}{2\pi v_0^2}\right)^{1/2}\frac{s^{-1}-1}{s^{-2}+p-1}\exp\left[-\frac{(p+2)v_\parallel^2}{2v_0^2}\right]. \tag{4.8}$$

This is the sum of two Gaussians and is plotted in Fig. 3(d) (dashed line). The mean line-of-sight velocity is zero and the dispersion σ_{los} is $0.492v_0$. Notice that both (4.7) and (4.8) reduce to (3.15) in the limit $s=1$, as of course they should.

Table 1. Properties of the anisotropic composite models.

Mass, M	$2^{p-3}B(\frac{p-3}{2},\frac{p-3}{2})\pi\rho_0 qR_c^3\frac{p+2(s^{-2}-1)}{p(p-2)}$
Kinetic Energy, T	$\frac{Mv_0^2}{2(p+2)}\frac{(4s^{-2}-1)p+6}{p+2(s^{-2}-1)}$
Virial, Ω	$-\frac{Mv_0^2}{(p+2)}\frac{(4s^{-2}-1)p+6}{p+2(s^{-2}-1)}$
Edge-On Surface Brightness, $I(x',y')$	$2^{p-2}B(\frac{p-1}{2},\frac{p-1}{2})\rho_0 R_c^p\frac{[ps^{-2}x'^2+(s^{-2}+p-1)(R_c^2+q^{-2}y'^2)]}{p[x'^2+R_c^2+q^{-2}y'^2]^{(p+1)/2}}$
Edge-On Line of Sight Second Moment, $\langle v_{los}^2\rangle(x',y')$	$\frac{v_0^2}{p}+\frac{2v_0^2(s^{-2}-1)}{p(p+2)}\times\frac{[x'^2(p^2-4p+2)-R_c^2-q^{-2}y'^2]}{[ps^{-2}x'^2+(s^{-2}+p-1)(R_c^2+q^{-2}y'^2)]}$

The distribution function of the maximum streaming model is again found by reversing the directions of the clockwise rotating stars. The maximum streaming velocity is

$$\langle v_\phi \rangle = v_0 \left(\frac{2}{\pi p}\right)^{1/2} \left[1 + \frac{(2\sqrt{p} - \sqrt{p+2})}{\sqrt{p+2}} \frac{(s^{-2}-1)R^2}{R_c^2 + s^{-2}R^2 + q^{-2}z^2}\right]. \tag{4.9}$$

The corresponding line profile can again be written down as a rather lengthy but single quadrature over error functions. It is plotted in Fig. 3(d) (dot–dashed line).

5 CONCLUSIONS

The self-consistent distribution function that generates the axisymmetric logarithmic potential of Binney is found. The distribution function depends only on the binding energy E and component of angular momentum parallel to the symmetry axis L_z. There is no globally defined isolating third integral of motion and so this is the simplest (even part of the) steady-state distribution function. The phase space density is everywhere positive if, and only if, the axial ratio of the spheroidal equipotentials q satisfies $0.707 \leqslant q \leqslant 1.08$.

It is astrophysically more realistic to synthesize composite models with a luminous component and a dark halo. The dark and shining matter together generate the potential–density pair of Binney's model. Taking the distribution function of the stars as an isothermal gives *the simplest known axisymmetric galaxy models.* Of course, the distribution function of the dark matter is found by subtracting the isothermal from the full distribution function of Binney's model to yield an entirely self-consistent solution of the Poisson and Vlasov equations. The luminosity density is stratified on similar concentric spheroids and possesses any asymptotic density fall-off. The surface brightness is a reasonably good fit to the de Vaucouleurs profile. The isothermal composite models cannot get flatter than E3. This defect may be remedied by modifying the distribution function of the luminous component to accentuate the density in the equatorial plane. This yields oblate mass models as flat as E6 with anisotropic kinematics embedded within the dark halo. All the models are sufficiently simple to enable the rather awkward triple integral for the line profile to be reduced to a single quadrature and evaluated swiftly and accurately on the computer.

It is interesting to extend this work by examining the lowered isothermal model corresponding to the axisymmetric logarithmic potential. The distribution function is modified from (2.4) to

$$F = \begin{cases} AL_z^2[\exp(4E/v_0^2) - 1] + B[\exp(4E/v_0^2) - 1] + C[\exp(2E/v_0^2) - 1], & \text{if } E \leqslant 0, \\ 0, & \text{if } E > 0, \end{cases} \tag{5.1}$$

where we have exploited an arbitrary constant to set the critical relative binding energy to zero at the truncation radius. This is of course an axisymmetric extension of the well-known models introduced by Michie & King (Michie 1963; King 1966). The Poisson equation must now be solved numerically. Near the core, the models are very like the axisymmetric logarithmic potential – but they have the advantage of finite total mass. Another useful generalization is to examine density components of the form

$$\rho_{\text{luminous}} = \frac{\rho_0 R_c^p}{(R_c^2 + R^2 + s^{-2}z^2)^{p/2}}. \tag{5.2}$$

These are spheroidal components like those studied in Section 3, but without the restriction that they coincide with the global equipotentials ($s \neq q$). It is not possible to find the distribution function analytically, but it can be done numerically using the powerful methods developed by Hunter & Qian (1993). This enables the construction of very realistic galaxy models with bulge, thick disc and halo.

Axisymmetric galaxy models with simple distribution functions are exceedingly rare. Indeed, axisymmetric models with any kind of distribution function – no matter simple – are rare! No doubt this is partly because insufficient attention has been bestowed on the problem. Work in progress aims to give a systematic algorithm for finding simple axisymmetric models, as well as to provide galactic astronomers with a tool-box of usable distribution functions for galaxies with dark haloes, central cusps and black holes.

ACKNOWLEDGMENTS

This work was started while visiting the Huygens Laboratorium, Leiden, whose hospitality is gratefully acknowledged. The visit was made possible by a grant from the Leids Kerkhoven Bosscha Fonds. Conversations with Donald Lynden-Bell, Tim de Zeeuw, Chris Hunter, Ortwin Gerhard, Enping Qian, Roeland van der Marel and Simon White were extremely fruitful. Alar Toomre is thanked for a stimulating correspondence, as well as for pointing out an error in the preprint version. NWE is supported by a research fellowship from King's College, Cambridge.

REFERENCES

Binney J. J., 1981, MNRAS, 196, 455
Binney J. J., 1988, in Corwin H. G., Bottinelli L., eds, The World of Galaxies. Springer-Verlag, New York, p. 332
Binney J. J., Tremaine S., 1987, Galactic Dynamics. Princeton University Press, Princeton, Ch. 2, 3
Contopoulos G., 1954, Z. Astrophys., 35, 67
Dejonghe H., 1986, Phys. Rep., 133, 218
de Vaucouleurs G., 1948, Ann. Astrophys., 11, 247
Hubble E. P., 1930, ApJ, 71, 231
Hunter C., 1975, AJ, 80, 783
Hunter C., Qian E., 1993, MNRAS, submitted
Illingworth G. D., Franx M., 1989, in Merritt D., ed., Dynamics of Dense Stellar Systems. Cambridge University Press, Cambridge, p. 13
Jaffe W., 1987, in de Zeeuw P. T., ed., Structure and Dynamics of Elliptical Galaxies. Reidel, Dordrecht, p. 511
King I. R., 1966, AJ, 71, 64
Kormendy J., 1977, ApJ, 218, 333
Lake G., 1981, ApJ, 243, 111
Lynden-Bell D., 1960, MNRAS, 120, 204
Lynden-Bell D., 1962, MNRAS, 123, 447
Michie R. W., 1963, MNRAS, 125, 127
Rood H., Page T., Kintner E., King I., 1972, ApJ, 175, 627
Toomre A., 1982, ApJ, 259, 535

APPENDIX A: THE POSITIVITY OF THE DISTRIBUTION FUNCTIONS OF THE COMPOSITE MODELS

In this appendix, the necessary and sufficient conditions for the phase space density of the distribution functions of the dark and the stellar matter to be positive definite are given in the instance $q \leqslant 1$. They are straightforward, but a little cumbersome, to derive.

The obvious and sensible restriction that the mass densities of both components are positive already implies that the mass-to-light ratio $\Upsilon \geq 1$ everywhere. Imposing the positivity of phase space density yields more stringent conditions, which are compactly given in terms of the central mass-to-light ratio $\Upsilon(0, 0)$. For the isotropic composite models of Section 3, we must distinguish three cases. If $p = 2$, then

$$\Upsilon(0,0) \geq \frac{2q^2+1}{2q^2-1}. \tag{A1}$$

If $2 < p < 4$, the condition is

$$\Upsilon(0,0) \geq \frac{(2q^2+1)(4-p)^{(4-p)/2}(p-2)^{(p-2)/2}p^{3/2}}{(2q^2-1)^{(4-p)/2}2^{5p/4}}. \tag{A2}$$

Lastly, if $p \geq 4$, then

$$\Upsilon(0,0) \geq \frac{(2q^2+1)p^{3/2}}{2\sqrt{2}(4\sqrt{2}-1+2q^2)}. \tag{A3}$$

It is a helpful aid to understanding to calculate these restrictions for a particular model. Suppose we take $q = 0.80$ as the axis ratio of the spheroidal density contours, then with asymptotic decay $p = 2$, 3 and 4, the central mass-to-light ratio must exceed 8.14, 1.66 and 1.09 respectively. At least in the last two instances, the constraints are not markedly more restrictive than just asking for positive mass densities!

For the anisotropic composite models of Section 4, we must additionally impose that

$$\Upsilon(0,0) \geq \frac{(2q^2+1)(s^{-2}-1)(p+2)^{5/2}}{64(1-q^2)}. \tag{A4}$$

The example $p = s^{-2} = 3.5$ and $q = 0.80$ corresponds to a luminous component of ellipticity 0.440 and asymptotic density decay $r^{-3.5}$. The constraint implies the central mass-to-light ratio exceeds 17.6, which is now a good deal more than implied by positive mass density.